Morphable structures from unicellular organisms with active, shape-shifting envelopes: variations on a theme by Gauss

Giancarlo Cicconofri[a], Marino Arroyo[b], Giovanni Noselli[c], Antonio DeSimone[d,c,*]

[a] *GSSI–Gran Sasso Science Institute, viale Francesco Crispi 7, 67100 L'Aquila, Italy*
[b] *Universitat Politècnica de Catalunya, 08034 Barcelona, Spain*
[c] *SISSA–International School for Advanced Studies, via Bonomea 265, 34136 Trieste, Italy*
[d] *The BioRobotics Institute, Scuola Superiore Sant'Anna, viale Rinaldo Piaggio 34, 56025 Pontedera, Italy*

Abstract

We discuss some recent results on biological and bio-inspired morphing, and use them to identify promising research directions for the future. In particular, we consider issues related to morphing at microscopic scales inspired by unicellular organisms. We focus on broad conceptual principles and, in particular, on morphing approaches based on the use of Gauss' *theorema egregium* (Gaussian morphing). We highlight some connections with biological cell envelopes containing filaments and motors, and discuss ideas for the implementation of Gaussian morphing in surfaces actuated by active shearing or stretching.

Keywords: deployable structures, soft robotics, cell motility, Gaussian morphing, active shells, unicellular swimmers, micro-swimmers, fluid-structure interaction

1. Introduction

Interest in shape-shifting structures has clear motivations and a relatively long history. Bimetallic strips, plates or shells, used as temperature-activated morphable structures (thermostats) provide but one popular example. They have been modeled in the linear response regime in the pioneering paper Timoshenko (1925), more recently in the nonlinear regime in Freund (2000), and have been used innumerable times, for example in the dome-shaped electric kettle switches by Taylor (2019). A variant of this idea, namely, exploiting conformational changes for functional adaptation is provided by deployable structures. Here the conformation in the translocation phase is as compact as possible to minimize transportation costs (broadly interpreted), while conformation during the service phase satisfies different functional requirements. Arrays of solar panels for harvesting solar energy in space provide one example: they need to be compactly folded to be launched by satellite rockets, they have to maximize area for maximal energy collection when in orbit Pellegrino (2018). But exactly the same idea applies equally well to biomedical devices such as stents. Valuable information on the mechanics of deployable structures is in Pellegrino (2001).

More recently, the problem of shape-shifting structures has acquired a biological twist, with a great perceived potential for new applications in bio-medical engineering. On the biology side, organisms use the possibility of changing conformation in many ways that are fundamental for biological functions. One of them is motility, and cell motility in particular, whose study has

*Corresponding author.
Email address: a.desimone@santannapisa.it (Antonio DeSimone)

been made possible by recent advances in microscopy techniques. The new observations now available provide us with a rich source of inspiration for novel shape-shifting mechanisms. One example comes from the study of the swimming strategies of unicellular organisms, from bacteria, to sperm cells, algae, microbes, and parasites, see *e.g.*, Taylor (1951); Lighthill (1975); Purcell (1977); Shapere and Wilczeck (1989); Lauga and Powers (2009); Drescher et al. (2010); Gaffney et al. (2011); Goldstein (2015); Rossi et al. (2017); Cicconofri and DeSimone (2016, 2019) and the references cited therein for a very conspicuous body of literature. Here, executing a shape change while immersed in a fluid is used to extract propulsive forces from the resistance that the fluid offers to the swimmer, which stirs the fluid around when it deforms its body. But the topic is much broader including, for example, the shape changes driven by the mitotic spindle when a cell divides Oriola et al. (2018).

While there is a clear biological interest in understanding the mechanisms by which nature has solved the problem of controlling shape at the micrometer scale, this topic is also of great appeal for bio-medical engineering applications. Here, a new generation of minimally invasive diagnostic and surgical tools could be designed based on concepts bio-inspired by the motility of cells and micro-organisms that proficiently navigate inside the human body Ornes (2017). Quoting Feynman (1960), it would be interesting in surgery if you could swallow your surgeon. Biological swimming and crawling have been studied extensively under this perspective, see *e.g.* Becker et al. (2003); Dreyfus et al. (2005); Menciassi et al. (2006); Feng and Cho (2014), and contributions from our own team include Alouges et al. (2011, 2013); DeSimone et al. (2013); Noselli and DeSimone (2014); DeSimone et al. (2015); Cicconofri and DeSimone (2015); Agostinelli et al. (2018); Alouges et al. (2019). More generally, the topic is of interest in Soft Robotics, a new paradigm in the design of robotic systems capable of operating outside the clean and predictable environment of a factory, having to deal with the challenges of unstructured environments, uneven terrains, unpredictable interactions with living beings and humans Kim et al. (2013).

Engineering structures are often thin and slender objects, with one dimension much smaller than the other two (2d membranes, plates, and shells) or two dimensions much smaller than the other one (1d rods). In these cases, shape control arises from control of curvature. In the 2d case, there are two main avenues to achieve this. The first one operates by inducing differential strains along the thickness, as in Timoshenko's bimetallic strips quoted above and in modern soft variants, see *e.g.* Sawa et al. (2010); DeSimone (2018); Caruso et al. (2018); Agostiniani et al. (2018). The second one operates by controlling in-plane stretches and exploiting Gauss' *theorema egregium*. This second avenue, based on the fact that Gaussian curvature is associated with derivatives of the components of the metric tensor, *i.e.*, differential stretches of the mid-surface, has received a lot of attention in the recent literature, see *e.g.*, Klein et al. (2007); Santangelo (2011); Modes and Warner (2015); Mostajeran (2015) and many others. We call *Gaussian morphing* this second strategy, namely, the idea of controlling curvature (shape) of a thin two-dimensional structure through modulated stretching of the mid-surface (via prescription of the metric tensor).

Many results are available on how this Gaussian morphing principle is at work in biological structures Shahaf et al. (2011); Aharoni et al. (2012); Arroyo et al. (2012); Arroyo and DeSimone (2014), and on how it can be exploited in artificial structures, *e.g.*, by using hydrogels or nematic elastomers Kim et al. (2012); Aharoni et al. (2014). But work is still required to move beyond the proof of concept stage, towards the reliable design and the accurate control of the response of shape-shifting active structures. It is our opinion, and the main point we wish to make in this paper, that this endeavor will benefit from a clearer appreciation of how the problem of shape control (both the so called direct problem of controlling shape, and the so called inverse problem of determining an actuation strategy capable of realizing a desired shape) is intimately linked to a notion of *embodiment*, namely, the specification of a concrete mechanism by which the change

of metric is enforced. In the absence of this ingredient, the problem is ill-defined. Our point of view on the subject has been shaped by working at the intersection of many diverse perspectives: understanding of biological organisms by quantitative mathematical modelling of the forces that they exert to control shape on one side, and, on the other side, the attempt to reproduce these mechanisms in concrete physical prototypes by using modern manufacturing techniques.

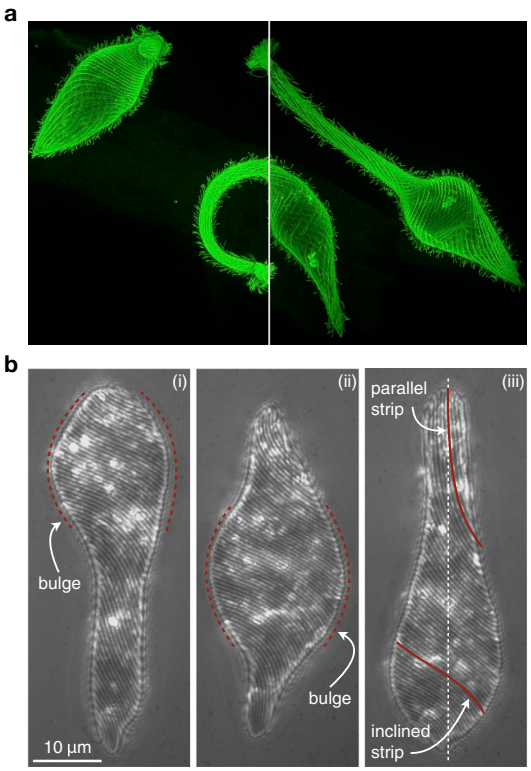

Figure 1: Neck protrusion and shape changes in the microtubule meshwork of *Lacrymaria olor* (top, reproduced with permission from Coyle et al. (2018)) and sliding helices in *Euglena gracilis* metaboly (bottom, adapted from Noselli et al. (2019a)).

In this paper, we discuss Gaussian morphing within the context of structures whose outer boundary consists of (is made of or, possibly, is activated by) a network of 1d filaments. From the biological point of view, this is the paradigm by which the cell envelope contains systems resulting from mixtures of filaments and motors (for example: acto-myosin cortex in eukaryotic cells, microtubule bundles and motors in eukaryotic flagella, motors with microtubule and pellicle strips in euglenids, and in *Euglena gracilis* in particular) or it simply consists of complex networks of filaments, whose shape is possibly controlled by other mechanisms, as in *Lacrymaria olor*, see Figure 1. From the point of view of engineered structures, we explore axisymmetric Gaussian morphing in structures made possible by different activation mechanisms, which we describe as changes of metric of shearing and of stretching type. The shearing mechanism is explored with an eye to structures made of sliding flexible strips in Noselli et al. (2019a). The stretching mechanism is analyzed for the possible connections with the braided sheaths used in McKibben pneumatic artificial muscles, see *e.g.* Tondu (2012) for a review of the underlying mechanical principles.

Finally, by modeling eukaryotic flagella as active tubular shells, we discuss how flagellar beating can be described as an instance of the Gaussian morphing principle. This is one of the new results contained in this paper, see Section 7. Indeed, eukaryotic flagella are typically described in the current biophysical literature as active rods, rather than as active shells. Another novelty in this paper is an expanded list of easy-to-use formulas that link actuation strain (stretching or shear) to emerging Gaussian curvature (hence shape), in particular in the axi-symmetric case, see equations (12), (13) and (14), the last two of which are new. We use these formulas to show in some concrete examples that the same shape changes can be obtained by prescribing different deformations of the material fibers making up the active surface. We conclude that, in discussing problems of shape control, one crucial ingredient is the specification of the mechanism by which the changes of the metric tensor are enforced, *i.e.*, the embodiment of the Gaussian morphing principle.

2. Gaussian morphing: controlling shape of surfaces by prescribing their metric

We start by considering the reference configuration of a material surface, namely, a two-dimensional surface immersed in $\mathbb{R}^3$ and its deformations. This means that we consider a map $(u,v) \mapsto \boldsymbol{\chi}_0(u,v) \in \mathbb{R}^3$, where $(u,v) \in (L_0, H_0) \subset \mathbb{R}^2$. A deformed configuration of this material surface will be given by another map, say, $(u,v) \mapsto \boldsymbol{\chi}(u,v) \in \mathbb{R}^3$, again with $(u,v) \in (L_0, H_0) \subset \mathbb{R}^2$.

By computing the surface deformation gradient $\boldsymbol{F}$ and the right Cauchy-Green strain $\boldsymbol{C} = \boldsymbol{F}^T\boldsymbol{F}$, we obtain the metric tensors of the material surface in the reference and deformed configurations as

$$\boldsymbol{C}_0 = g_0 = \begin{bmatrix} \boldsymbol{\chi}_{0,u}\cdot\boldsymbol{\chi}_{0,u} & \boldsymbol{\chi}_{0,u}\cdot\boldsymbol{\chi}_{0,v} \\ \boldsymbol{\chi}_{0,u}\cdot\boldsymbol{\chi}_{0,v} & \boldsymbol{\chi}_{0,v}\cdot\boldsymbol{\chi}_{0,v} \end{bmatrix} \tag{1}$$

and

$$\boldsymbol{C} = g = \begin{bmatrix} \boldsymbol{\chi}_{,u}\cdot\boldsymbol{\chi}_{,u} & \boldsymbol{\chi}_{,u}\cdot\boldsymbol{\chi}_{,v} \\ \boldsymbol{\chi}_{,u}\cdot\boldsymbol{\chi}_{,v} & \boldsymbol{\chi}_{,v}\cdot\boldsymbol{\chi}_{,v} \end{bmatrix} = \begin{bmatrix} E & F \\ F & G \end{bmatrix}, \tag{2}$$

where a comma denotes partial differentiation.

We are interested in inducing controlled changes of the shape of the material surface by generating changes of lengths and angles of its material fibers through actuation, described by changes of the metric tensor from its reference value g_0 to a new value g. The possibility of changing curvature (morphing) of a surface by acting on its metric is recognized by a remarkable theorem by Gauss, his celebrated *theorema egregium*, stating that the Gaussian curvature K of a surface (the product of its principal curvatures) can be computed by differentiating the components of its metric tensor as

$$-EK = (\Gamma^2_{12})_{,u} - (\Gamma^2_{11})_{,v} + \Gamma^1_{12}\Gamma^2_{11} + \Gamma^2_{12}\Gamma^2_{12} - \Gamma^2_{11}\Gamma^2_{22} - \Gamma^1_{11}\Gamma^2_{12}\,, \tag{3}$$

where $\Gamma^\alpha_{\beta\gamma}$, $\alpha,\beta,\gamma = 1,2$, are the Christoffel symbols, see do Carmo (1976). The interpretation of Gauss' theorem as a morphing scheme is contained in the pioneering work Klein et al. (2007).

We will discuss examples that are motivated by shape changes exhibited by unicellular organisms (cell motility). These can be interpreted as the result of changes of the metric of the material surface that describes their cell envelope. Progress in the available manufacturing techniques is starting to enable us to replicate these morphing mechanisms in prototypes, so that Gauss theorem can become a tool to engineer deployable or shape-shifting structures (Gaussian morphing), in particular those which are inspired by biological organisms (bio-inspired Gaussian morphing). Since shells can exhibit high stiffness thanks to the high resistance (by stretching) to

loads trying to modify their Gaussian curvature (resistance by shape) this also opens up the way to the design of structures whose stiffness properties can be tuned according to needs (adaptable structures).

One example of the paradigm just illustrated, analyzed in detail in Arroyo et al. (2012); Arroyo and DeSimone (2014); Noselli et al. (2019b,a), is a local simple shear arising from the sliding of pellicle strips making up the cell envelope of euglenids, namely

$$g = \begin{bmatrix} 1+\gamma^2 & \gamma \\ \gamma & 1 \end{bmatrix} \qquad \text{(shearing mechanism)}. \tag{4}$$

Here $\gamma = \gamma(u, v) \in \mathbb{R}$ is the local simple shear between material fibers aligned with the coordinate lines (the direction of the centerline of the pellicle strips in the case of euglenids), an area preserving deformation. The same mechanism powers flagellar and ciliary beating in eukaryotic cells, where molecular motors induce relative sliding between parallel bundles of microtubules arranged in space along the outer cylindrical envelope of the flagellum (the distinctive $9 + 2$ structure, which is highly conserved across all eukaryotic organisms, see Alberts et al. (2014)). Substituting (4) into (3) we obtain

$$K = \left(\gamma_{,u} - \gamma\gamma_{,v}\right)_{,v} \qquad \text{(shearing mechanism)}. \tag{5}$$

Another example, motivated by observations of the deformations of *Lacrymaria olor* in Coyle et al. (2018), is also at work in the braided sheaths of pneumatic artificial muscles of McKibben type Tondu (2012). It consists of a stretch with principal directions along the coordinate lines

$$g = \begin{bmatrix} \lambda^2 & 0 \\ 0 & \mu^2 \end{bmatrix} \qquad \text{(stretching mechanism)}, \tag{6}$$

where $\lambda = \lambda(u, v) \in (0, +\infty)$ and $\mu = \mu(u, v) \in (0, +\infty)$ are the stretches along the $u-$ and $v-$coordinate lines, respectively. These are typically the diagonals in the rhombus-shaped unit cell of a meshwork which deforms as a pantograph in the sheath of a McKibben or in an array of biofilaments in the cell envelope. It is conceivable to use the same mechanism actively, in order to induce the corresponding shape changes in an active shape-shifting engineered surface.

The deformation associated with (6) is area preserving if $\lambda\mu = 1$, in which case it is called a pure shear. Substituting (6) into (3) we obtain

$$K = -\frac{1}{\lambda\mu}\left(\left(\frac{\lambda_{,v}}{\mu}\right)_{,v} + \left(\frac{\mu_{,u}}{\lambda}\right)_{,u}\right) \qquad \text{(stretching mechanism)} \tag{7}$$

in the general case while, in the area-preserving case, we have

$$K = -\left(\lambda\lambda_{,v}\right)_{,v} - \left(\mu\mu_{,u}\right)_{,u} \qquad \text{(stretching mechanism}\,,\ \lambda\mu = 1). \tag{8}$$

3. Gaussian morphing of axisymmetric surfaces

We focus now on axisymmetric shape-shifting surfaces. As reference configuration S_0, we consider the cylinder of radius R_0 such that

$$\boldsymbol{\chi}_0(u, v) = \left\{R_0 \cos\left(\frac{u}{R_0}\right), R_0 \sin\left(\frac{u}{R_0}\right), v\right\}, \quad u \in (0, L_0), v \in (0, H_0)\,, \tag{9}$$

where $L_0 = 2\pi R_0$. This has the identity matrix as metric tensor g_0 and zero Gaussian curvature $K_0 = 0$, in agreement with formulas for g and K in the previous section obtained by setting either $\gamma = 0$ or $\lambda = \mu = 1$.

We are then interested in deformed configurations with axisymmetric shape S, which can be written by assigning a generating curve $\{r(v), z(v)\}$ in the symmetry plane and an azimuthal displacement $\psi(v)$, leading to

$$\boldsymbol{\chi}(u,v) = \left\{ r(v)\cos\left(\frac{u}{R_0}+\psi(v)\right), r(v)\sin\left(\frac{u}{R_0}+\psi(v)\right), z(v)\right\},\ u\in(0,L_0), v\in(0,H_0)\,. \quad (10)$$

Substituting (10) into (2) we obtain

$$\begin{bmatrix} (r/R_0)^2 & r^2\psi'/R_0 \\ r^2\psi'/R_0 & r'^2+z'^2+r^2\psi'^2 \end{bmatrix} = \begin{bmatrix} E & F \\ F & G \end{bmatrix} = g\,, \quad (11)$$

where a prime $(\cdot)'$ denotes differentiation with respect to v. Clearly, since the left hand side in the last equation depends only on v, only metric tensors $g = g(v)$ that are independent of u (axi-symmetric actuation) are compatible with (10). In these circumstances, equations (5), (7), and (8) from the last section simplify to

$$K = -\left(\gamma\gamma_{,v}\right)_{,v} \quad \text{(shearing mechanism)}, \quad (12)$$

$$K = \frac{1}{\lambda\mu}\left(\frac{1}{\mu^2}\lambda_{,v}\mu_{,v} - \frac{1}{\mu}\lambda_{,vv}\right) \quad \text{(stretching mechanism)}, \quad (13)$$

$$K = -\left(\lambda\lambda_{,v}\right)_{,v} \quad \text{(stretching mechanism, } \lambda\mu = 1), \quad (14)$$

respectively.

We would like to compute the axisymmetric shapes that can result from axisymmetric actuation patterns either in simple shear, $\gamma = \gamma(v)$, or in pure shear $\lambda = \lambda(v), \lambda\mu = 1$. From equation (11) we immediately see that, since $E = (r/R_0)^2$, whenever the metric g is constant, then the axisymmetric surface $\boldsymbol{\chi}$ is a cylinder of radius $r = E^{1/2}R_0$, a special instance of a surface with zero Gaussian curvature $K = 0$. This case of constant metric g is the simplest to examine, and we shall consider this case first.

4. Cylinders from cylinders

When $K = K_0 = 0$, the axisymmetric morphing surface can be developed onto a plane both before and after actuation. Following Arroyo and DeSimone (2014), in order to study the shape change $S_0 \mapsto S$ induced by the change of metric $g_0 \mapsto g$, it is useful to analyze the process by first cutting S_0 along a direction parallel to the cylinder axis and unfolding it (isometrically) to a plane, then deform this plane with a two-dimensional affine map $\boldsymbol{\Phi}(u,v)$ inducing the (spatially uniform) change of metric $g_0 \mapsto g$

$$\begin{bmatrix} \boldsymbol{\Phi}_{,u}\cdot\boldsymbol{\Phi}_{,u} & \boldsymbol{\Phi}_{,u}\cdot\boldsymbol{\Phi}_{,v} \\ \boldsymbol{\Phi}_{,u}\cdot\boldsymbol{\Phi}_{,v} & \boldsymbol{\Phi}_{,v}\cdot\boldsymbol{\Phi}_{,v} \end{bmatrix} = g = \begin{bmatrix} E & F \\ F & G \end{bmatrix}, \quad (15)$$

and then roll-up (isometrically) the deformed plane on a cylinder of radius $r = E^{1/2}R_0$. The case associated with a shearing mechanism is

$$\boldsymbol{\Phi}(u,v) = \boldsymbol{R}^{\phi}_{\boldsymbol{e}_3}\left(u\boldsymbol{e}_1 + (v+\gamma u)\boldsymbol{e}_2\right)\,, \quad g = \begin{bmatrix} 1+\gamma^2 & \gamma \\ \gamma & 1 \end{bmatrix}, \quad (16)$$

where $\boldsymbol{R}^{\phi}_{\boldsymbol{e}_3}$ is a rotation with axis $\boldsymbol{e}_3$ and angle $\phi = \tan^{-1}(\gamma)$. Metrics of this type were considered and extensively studied in Arroyo et al. (2012); Arroyo and DeSimone (2014). Another notable

example is the case associated with a stretching mechanism, and is given by

$$\boldsymbol{\Phi}(u,v) = \lambda u \boldsymbol{e}_1 + \mu v \boldsymbol{e}_2\,, \quad g = \begin{bmatrix} \lambda^2 & 0 \\ 0 & \mu^2 \end{bmatrix}. \tag{17}$$

Substituting (17) into (11) we obtain

$$\begin{bmatrix} (r/R_0)^2 & r^2\psi'/R_0 \\ r^2\psi'/R_0 & r'^2 + z'^2 + r^2\psi'^2 \end{bmatrix} = \begin{bmatrix} \lambda^2 & 0 \\ 0 & \mu^2 \end{bmatrix} = \text{constant}, \tag{18}$$

which gives $r = \lambda R_0$, while the functions $\psi(v)$ and $z(v)$ are determined by solving the differential equations

$$\psi' = 0\,, \tag{19}$$

and

$$z' = \pm\mu\,. \tag{20}$$

Hence, by setting the integration constants $\psi(0)$ and $z(0)$ equal to zero and selecting the plus sign in (20) (solutions to (18) are determined up to a rigid motion allowing for translations along $\mathbf{e}_3$, rotations about $\mathbf{e}_3$, and $\pm$ inversion along $\mathbf{e}_3$, which are here fixed), we have $\psi(v) = 0$ and $z(v) = \mu v$.

We are interested in the conformational changes of networks of material curves on S_0, when a metric change $g_0 \mapsto g$ transforms S_0 into S. We consider the $2N$ lines

$$u^{(k)}(v) = k\frac{2\pi}{N}R_0 \pm \tan(\vartheta_0)v\,, \quad k = 0, \dots, N-1 \tag{21}$$

and their images in the reference and deformed configurations

$$\begin{aligned} \boldsymbol{\chi}_0^{(k)}(v) &= \boldsymbol{\chi}_0(u^{(k)}(v), v) \\ &= \left\{ R_0 \cos\left(\frac{1}{R_0}u^{(k)}(v)\right), R_0 \sin\left(\frac{1}{R_0}u^{(k)}(v)\right), v \right\},\ v \in (0, H_0) \end{aligned} \tag{22}$$

and

$$\begin{aligned} \boldsymbol{\chi}^{(k)}(v) &= \boldsymbol{\chi}(u^{(k)}(v), z(v)) \\ &= \left\{ \lambda R_0 \cos\left(\frac{1}{R_0}u^{(k)}(v)\right), \lambda R_0 \sin\left(\frac{1}{R_0}u^{(k)}(v)\right), \mu v \right\},\ v \in (0, H_0). \end{aligned} \tag{23}$$

Curves (22) are circular helices with radius R_0, screw axis parallel to $\boldsymbol{e}_3$, and pitch angle ϑ_0. Curves (23) are circular helices with radius λR_0, screw axis parallel to $\boldsymbol{e}_3$, and pitch angle $\tan^{-1}(\lambda\tan(\vartheta_0)/\mu)$ (when $\vartheta_0 = \pi/4$, the angular pitch of (23) is $\tan^{-1}(\lambda/\mu)$). These are all illistrated in Figure 2.

5. Axisymmetric surfaces with non-constant metric

We turn now to more general axisymmetric surfaces S of the form (10), obtained by axisymmetric actuation, *i.e.*, by nonconstant metrics g depending only on the "vertical" coordinate v (the coordinate along the symmetry axis) and not on the "azimuthal" coordinate u. The case of simple shear (4) has been discussed in detail in Arroyo and DeSimone (2014). In fact, metrics of this type were considered in Arroyo et al. (2012); Arroyo and DeSimone (2014) and extensively studied in Arroyo et al. (2012); Arroyo and DeSimone (2014); Noselli et al. (2019b,a)

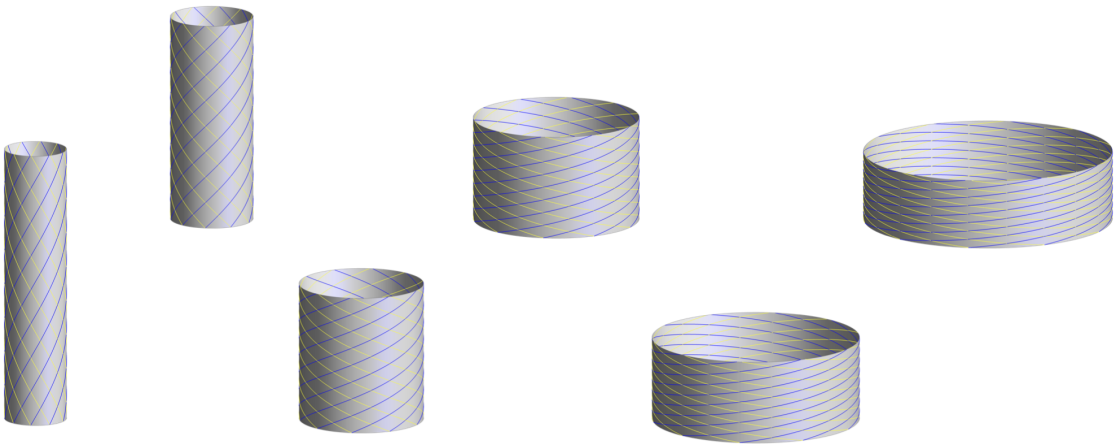

Figure 2: Cylindrical surfaces obtained from a referential cylinder with $H_0/R_0 = 5$ by exploiting the area preserving stretching morphing principle for $\lambda = \{0.75, 1, 1.5, 2, 2.5, 3\}$. Cylindrical surfaces are decorated by blue and yellow material fibers for $\theta_0 = \pi/4$ and $N = 10$.

in connection with the morphing mechanism of the pellicle of euglenids. In particular, Arroyo and DeSimone (2014) give the complete atlas of the axisymmetric shapes of constant Gaussian curvature surfaces (cylinders, cones, spheres, spindles, and pseudo-spheres) achievable by axisymmetric shearing, and solve the inverse problem of finding which shear actuation patterns, *i.e.*, which metric of the type (16), are capable of realizing each given shape.

Here, we consider the metric given by (6), restricting attention to the area-preserving case of $\lambda\mu = 1$ (pure shear) for simplicity. From

$$\begin{bmatrix} (r/R_0)^2 & r^2\psi'/R_0 \\ r^2\psi'/R_0 & r'^2 + z'^2 + r^2\psi'^2 \end{bmatrix} = \begin{bmatrix} \lambda^2 & 0 \\ 0 & 1/\lambda^2 \end{bmatrix}, \tag{24}$$

where $\lambda = \lambda(v)$ and a prime denotes derivative with respect to v, we obtain

$$r(v) = \lambda(v) R_0\,, \tag{25}$$

$$\psi'(v) = 0\,, \tag{26}$$

and

$$z'(v) = \pm\frac{1}{\lambda(v)}\sqrt{1 - (R_0\lambda\lambda')^2}\,, \tag{27}$$

which can be solved with real $z(v)$ provided that

$$\lambda|\lambda'| \leq \frac{1}{R_0}\,. \tag{28}$$

This is a necessary condition for the embeddability of a metric of the form (6) in the axisymmetric case.

We start by seeking surfaces of zero Gaussian curvature $K = 0$, more general than the cylinders of the previous section, which arise when $\lambda' = 0$. We thus have

$$0 = -(\lambda\lambda')' = -\frac{1}{2}(\lambda^2)''\,, \tag{29}$$

which implies that $\lambda(v)\lambda'(v) = C$, a constant such that $|C| \leq 1/R_0$. Hence,

$$z'(v) = \frac{dz}{dv} = \pm \frac{1}{\lambda(v)} \sqrt{1 - R_0^2 C^2} \tag{30}$$

and, using (25), we deduce that

$$\frac{dr}{dz} = \frac{\frac{dr}{dv}}{\frac{dz}{dv}} = \pm \frac{R_0 \lambda(v)\lambda'(v)}{\sqrt{1 - R_0^2 C^2}} = \pm \sqrt{\frac{R_0^2 C^2}{1 - R_0^2 C^2}} =: \pm \tan(\phi)\,, \tag{31}$$

which shows that S is a cone with axis parallel to $\boldsymbol{e}_3$ and opening angle ϕ (measured clockwise from the $\boldsymbol{e}_3$ axis). This angle tends to zero when $C \to 0$, and to $\pi/2$ when $C \to \pm 1/R_0$.

Moreover, it follows from (29) that $\lambda^2(v)$ is a linear function of $v \in (0, H_0)$. Thus, we can write λ as

$$\lambda = \tilde{\lambda}(\xi) = \sqrt{A(1-\xi) + B\xi}\,, \quad \xi := \frac{v}{H_0} \in (0,1)\,, \quad \tilde{\lambda}(0) = \sqrt{A}\,, \quad \tilde{\lambda}(1) = \sqrt{B} \tag{32}$$

and integrate (30) to obtain

$$z(v) = z(0) \pm H_0 \sqrt{1 - R_0^2 C^2} \int_0^{v/H_0} \frac{dx}{\sqrt{A(1-x) + Bx}}\,. \tag{33}$$

Furthermore, from $\lambda\lambda' = (\lambda^2)'/2 = C$, we obtain

$$C = \frac{B - A}{2H_0}\,, \tag{34}$$

so that the embeddability condition $|C| \leq 1/R_0$ is equivalent to

$$|B - A| - \frac{2H_0}{R_0} \leq 0\,. \tag{35}$$

Setting all the integration constants to zero and choosing the positive sign in the previous formulas, we obtain the parametrization of S as

$$\lambda(v) = \sqrt{A\left(1 - \frac{v}{H_0}\right) + B\frac{v}{H_0}}\,, \tag{36}$$

$$r(v) = \lambda(v) R_0\,, \tag{37}$$

$$\psi(v) = 0\,, \tag{38}$$

and

$$z(v) = \frac{\sqrt{A(1 - R_0^2 C^2)}}{C} \left(\sqrt{1 - \frac{v}{H_0} + \frac{B}{A}\frac{v}{H_0}} - 1 \right), \tag{39}$$

which describes a truncated cone with opening angle given by (31) and radii at the rim of the surface equal to $r(0) = R_0\sqrt{A}$ and $r(H_0) = R_0\sqrt{B}$. Here $A = \lambda^2(0)$, $B = \lambda^2(H_0)$, $C = (B - A)/(2H_0)$ and A, B must be such that $|B - A| - 2H_0/R_0 \leq 0$.

The images of the circular helices (22) after deformation are obtained by substituting the previous formulas into

$$\begin{aligned}\boldsymbol{\chi}^{(k)}(v) &= \boldsymbol{\chi}(u^{(k)}(v), z(v)) \\ &= \left\{ r(v)\cos\left(\frac{1}{R_0}u^{(k)}(v)\right), r(v)\sin\left(\frac{1}{R_0}u^{(k)}(v)\right), z(v)\right\},\ v \in (0, H_0)\end{aligned} \tag{40}$$

and are represented in Figure 3.

Figure 4 shows a comparison between surfaces and networks of material lines arising form the two different actuation mechanisms. The figure shows that the same shapes can be obtained with two different metrics (one corresponding to a stretching mechanism, the other one to a shearing mechanism). The two mechanisms (not the shapes) are distinguishable because they lead to different deformations of the networks of material lines, and lead to different displacements of material points on the surfaces. The difference, however, is not without subtleties. For each fixed value γ of the shearing metric g, there is a stretching metric delivering the same shape, through stretches along different coordinate lines, the ones along the γ-dependent eigenvectors of g. A change of coordinates transforms one metric into the other. If, however, we insist on the fact that some curves in the reference configuration have the character of material lines, and that the embodiment of the shape-shifting mechanism governs the change of lengths and angles of material lines, then the two mechanisms by shearing and stretching are no longer interchangeable: The embodiment reveals the difference between the two mechanisms. A more complete discussion of this issue, and a more complete characterization of the available shapes (direct problem) and of the actuation patterns needed to produce them (inverse problem) will be provided elsewhere.

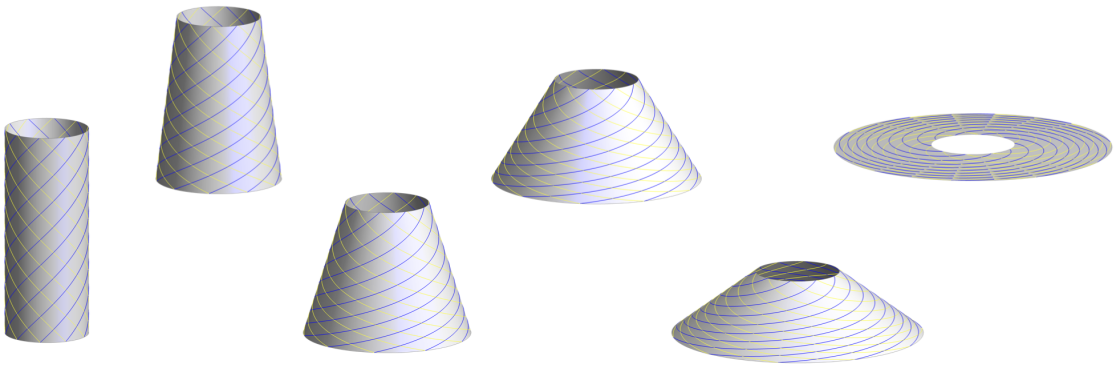

Figure 3: Truncated cones obtained from a referential cylinder with $H_0/R_0 = 5$ by exploiting the stretching morphing principle for $r(0)/R_0 = \{1, 1.5, 2, 2.5, 3, 3.32\}$ and $r(H_0)/R_0 = 1$. Conical surfaces are decorated by blue and yellow material fibers for $\theta_0 = \pi/4$ and $N = 10$.

6. Localized bulges

Of particular interest is the construction of localized axisymmetric bulges. These have been used in the context of the shearing activation mechanism to mimic the travelling peristaltic waves rationalizing metaboly (also known as amoeboid motion) in Euglenids Arroyo and DeSimone (2014); Noselli et al. (2019b). Here, we consider the following variant in the context of the

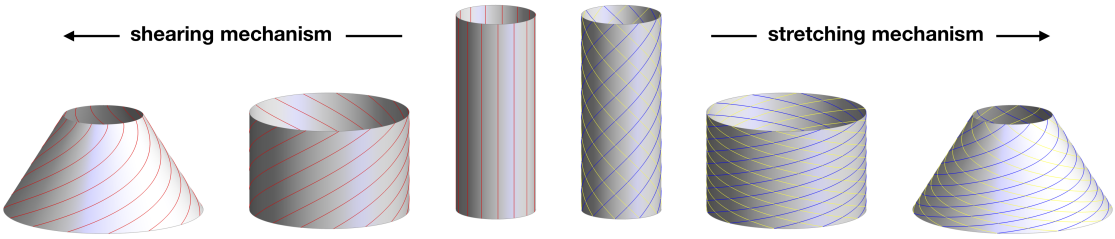

Figure 4: A comparison between identical shapes (cylinders and truncated cones) obtained by means of either a shearing (left) or stretching (right) mechanism. All the shapes are for $H_0/R_0 = 5$. The shorted cylinders correspond to $\gamma = \sqrt{3}$ (shearing mechanism) and to $\lambda = 2$ (stretching mechanism). Cones are both such that $r(0)/R_0 = 2.5$ and $r(H_0)/R_0 = 1$. Surfaces are decorated by colored material fibers to highlight the *embodiment* of the morphing principle and to emphasize the difference between the two morphing mechanisms.

stretching activation mechanism

$$\tilde{\lambda}(\xi) = 1 + A\left(1 - \exp\left[-\left(\frac{\xi - \xi_0}{D}\right)^2\right]\right), \quad \xi := \frac{v}{H_0} \in (-1, 1)\,, \tag{41}$$

where $A > -1$ determines the strength of the bulge perturbation with respect to the reference cylinder (9), $D > 0$ determines its non-dimensional breadth, and both satisfy embeddability constraints, while $\xi_0 \in (-1, 1)$ locates the centre of the bulge along the symmetry axis.

The shapes resulting from (41) are shown in Figure 5. They are closely reminiscent of the patterns exhibited by the unicellular predator *Lacrymaria olor* when it protrudes its neck for feeding, see Figure 1. Shape changes of a similar kind are also exhibited by *Euglena gracilis* executing metaboly, even though the extent of the protrusions is less extreme. There, the activation mechanism (the metric change) and the displacements of material points on the surface (the sliding pellicle strips) arise from a continuous one–parameter family of shears (12) rather than stretches (13), see Arroyo and DeSimone (2014); Noselli et al. (2019b). The details by which the two unicellular organisms control their behavior are still largely unknown.

7. Non-axisymmetric shapes

Finally, we consider a shape change which is not axisymmetric, in order to sketch a kinematic model for the axoneme, the slender bundle of microtubules that constitutes the internal scaffold of the eukaryotic flagellum Alberts et al. (2014). We emphasize that this structure is commonly represented as a rod with spontaneous curvature, or with internal shearing forces modeling the action of the molecular motors on the microtubules, see e.g. Camalet and Jülicher (2000). We represent it here as a tubular active shell, within the Gaussian morphing paradigm.

In this preliminary investigation, we focus on flagellar shapes in the absence of external loads. These are typically of hydrodynamic nature: equilibrium shapes of flagella beating in a fluid emerge from a force balance to which they contribute. This is discussed in several papers, for example in the seminal work by Machin (1958). Here we neglect external loads and treat microtubules as (inextensible) fibers on a tubular surface of radius R_0, see Figure 6. The centerline of the tubular surface is given by the curve $\mathbf{r}(\zeta)$, parametrized by its arc length ζ. For simplicity we restrict ourselves to centerlines lying on a plane

$$\mathbf{r}(\zeta) = \big\{r_x(\zeta), 0, r_z(\zeta)\big\}\,.$$

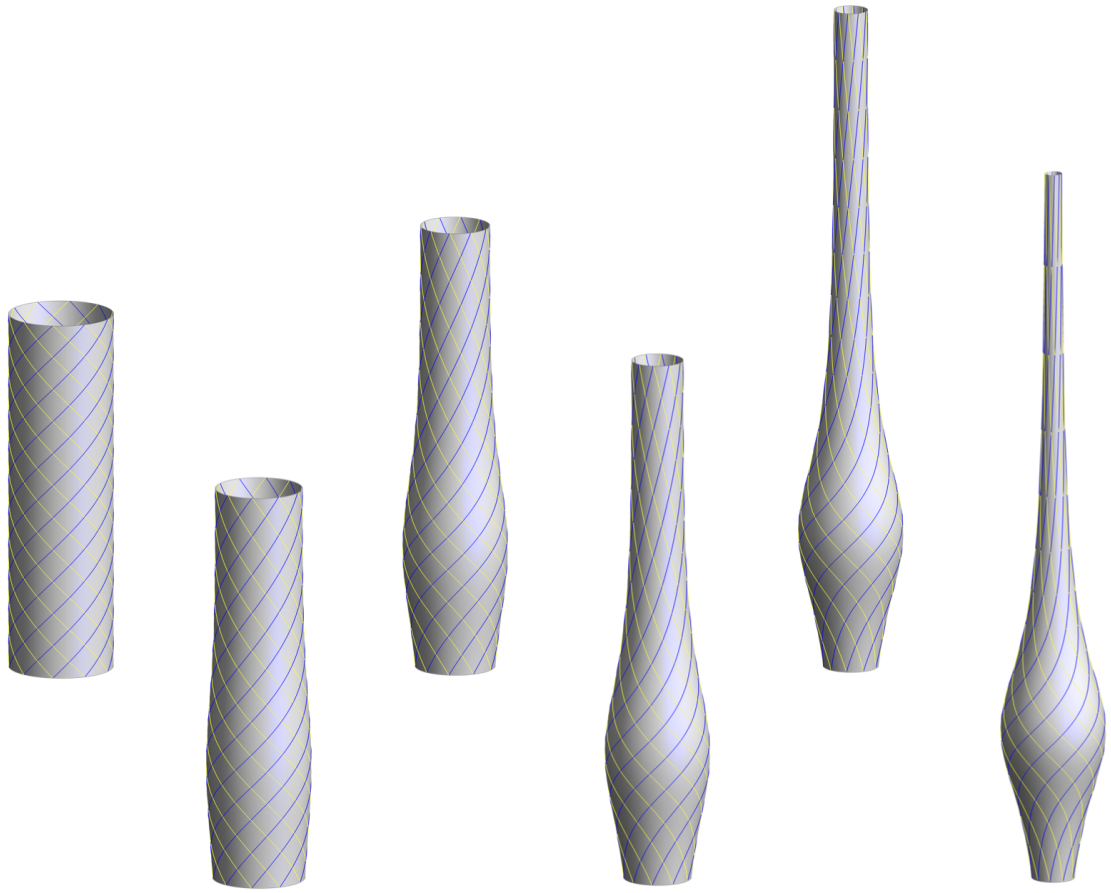

Figure 5: Extension of a neck resembling *Lacrymaria olor* obtained by means of the stretching mechanism from a cylinder. Shapes are obtained by exploiting Eq. (41) with $A = \{0, -0.17, -0.34, -0.51, -0.68, -0.85\}$, $D = 0.28$, and $\xi_0 = 0.3$. The referential cylinder is such that $H_0/R_0 = 7$. Surfaces are decorated by blue and yellow material fibers for $\theta_0 = \pi/4$ and $N = 10$.

Associated to the curve $\mathbf{r}(\zeta)$ we consider the orthonormal frame

$$\mathbf{d}_1(\zeta) = \{\cos\theta(\zeta), 0, \sin\theta(\zeta)\}\,, \quad \mathbf{d}_2(\zeta) = \{0,1,0\}\,, \quad \text{and} \quad \mathbf{d}_3(\zeta) = \{-\sin\theta(\zeta), 0, \cos\theta(\zeta)\}\,,$$

where $\mathbf{d}_3(\zeta) = \mathbf{r}_{,\zeta}(\zeta)$ is the centerline's unit tangent. The orthonormal frame $\{\mathbf{d}_1, \mathbf{d}_2, \mathbf{d}_3\}$ is completely determined by the angle θ between the centerline's tangent $\mathbf{d}_3$ and the z axis.

We use as a "template" for the axonemal outer surface the map

$$\boldsymbol{\psi}(\phi,\zeta) = \mathbf{r}(\zeta) + R_0\big(\cos\phi\,\mathbf{d}_1(\zeta) + \sin\phi\,\mathbf{d}_2(\zeta)\big) \tag{42}$$

depending on the generalized cylindrical coordinates ζ and ϕ. This surface is actually made of nine outer microtubules, which we assume to lie on the graph of the curves $\zeta \mapsto \boldsymbol{\psi}(\phi_k,\zeta)$ for $\phi_k = 2\pi k/9$ with $k = 1,2,\dots,9$. A reparametrization of (42) gives us the material configuration of the axonemal surface

$$\boldsymbol{\chi}(u,v) = \boldsymbol{\psi}\left(\frac{u}{R_0}, Z\left(\frac{u}{R_0}, v\right)\right), \quad u \in (0, L_0), \quad v \in (0, H_0)\,, \tag{43}$$

where $L_0 = 2\pi R_0$, H_0 is the microtubules' length, and where the function $Z(\phi, v)$ is defined (implicitly) by the equality

$$Z\big(\phi, V(\phi,\zeta)\big) = \zeta \quad \text{with} \quad V(\phi,\zeta) = \int_0^\zeta \|\boldsymbol{\psi}_{,\zeta}(\phi,\zeta')\|\,d\zeta'\,. \tag{44}$$

Notice that the graphs of the curves $\zeta \mapsto \boldsymbol{\psi}(\phi_k,\zeta)$ do not change under the reparametrization in (43). Moreover, from the definition of the function Z in (44) it follows that $G = \|\boldsymbol{\chi}_{,v}\|^2 = 1$, so microtubules are indeed inextensible.

Axonemes are slender structures, where for most systems we have $R_0/H_0 \sim 10^{-2}$. Taking $H_0 = 1$, we can exploit the fact that $R_0 \ll 1$ to obtain explicit approximate formulas for kinematic quantities of interest. Direct calculations from (42) and (44) give

$$V(\phi,\zeta) = \int_0^\zeta 1 + R_0\cos\phi\,\theta_{,\zeta}(\zeta')d\zeta' = \zeta + R_0\cos\phi\,\theta(\zeta)\,,$$

where we assumed $\theta(0) = 0$. From the previous calculation it follows that

$$Z(\phi, v) \approx v - R_0\cos\phi\,\theta(v)\,.$$

To verify the above equation we can simply check that the first equation in (44) is solved up to the first order in R_0. Plugging the approximated expression for Z in (43), and Taylor expanding in R_0 up to the first order, we obtain

$$\boldsymbol{\chi}(u,v) \approx \mathbf{r}(v) + R_0\Big(\cos\left(\frac{u}{R_0}\right)\big(\mathbf{d}_1(v) - \theta(v)\mathbf{d}_3(v)\big) + \sin\left(\frac{u}{R_0}\right)\mathbf{d}_2(v)\Big)\,.$$

Up to an error $\mathcal{O}(R_0)$, the tangent vectors to the material surface are given by

$$\boldsymbol{\chi}_{,u} \approx -\sin\left(\frac{u}{R_0}\right)\big(\mathbf{d}_1(v) - \theta(v)\mathbf{d}_3(v)\big) + \cos\left(\frac{u}{R_0}\right)\mathbf{d}_2(v) \quad \text{and} \quad \boldsymbol{\chi}_{,v} \approx \mathbf{d}_3(v)\,.$$

Direct calculations show that, at the same order of approximation, the metric tensor g associated with (43) has the form (4), with the shear function γ given by

$$\gamma(u,v) = \sin\left(\frac{u}{R_0}\right)\theta(v)\,. \tag{45}$$

Starting from the $\mathcal{O}(R_0)$ approximation of the outer unit normal

$$\mathbf{n} \approx \cos\left(\frac{u}{R_0}\right)\mathbf{d}_1(v) + \sin\left(\frac{u}{R_0}\right)\mathbf{d}_2(v)$$

we can calculate the Gaussian curvature K of the axonemal surface, from its standard (extrinsic) definition. At the leading order approximation, up to an error $\mathcal{O}(1)$, we obtain

$$K \approx \cos\left(\frac{u}{R_0}\right)\frac{\kappa(v)}{R_0}\,, \tag{46}$$

where $\kappa(v) = \theta_{,v}(v)$ is the centerline's curvature. It is straightforward to check that, at the same order of approximation, the expression for K coincides with the right hand side of (5), when γ is given by (45).

Formulas (45)-(46) show the relation between the relative sliding of microtubules and the geometry of the axonemal centerline. They state that, given a suitable microtubule shear pattern, the centerline of the axoneme can attain any (planar) shape. Indeed, γ directly defines the angle θ, which determines centerline curve $\mathbf{r}$ via the equation

$$\mathbf{r}_{,\zeta}(\zeta) = \big\{-\sin\theta(\zeta), 0, \cos\theta(\zeta)\big\}\,. \tag{47}$$

In Figure 6 we show a flagellar beat (one period of a periodic time history of axonemal surfaces) that mimics those of model organisms such as *Chlamydomonas reinhardtii* Goldstein (2015). An important feature of this beat is that it is periodic but non-reciprocal: the beat is divided into two distinct phases, namely, the power phase in which the flagellum is more extended and the recovery phase in which it is more compact. The lower hydrodynamic resistance characterizing the more compact shape of the recovery phase ensures the symmetry breaking necessary to the emergence of net displacements, even in the absence of inertia Purcell (1977).

As a final remark, we observe that (45) also highlights the following important aspect of flagellar beating. In order for a flagellum to bend, microtubules at opposite sides of the bending plane must have shears of opposite sign. That is, if for some fixed value of v we have $\gamma(u, v) > 0$ for $0 < u < \pi R_0$, then we must have $\gamma(u, v) < 0$ for $\pi R_0 < u < 2\pi R_0$. This observation led to the conclusion that there must exist some coordination mechanism between molecular motors acting on opposite sides of the flagellum. In order to generate flagellar beating, molecular motors must switch on and off, respectively, at the opposite sides of the bending plane. In the biophysical literature this is called the "switch-point hypothesis". What controls the switching of activation of axonemal motors is still a debated issue, and it is the subject of active ongoing research Lindemann and Lesich (2010); Lin and Nicastro (2018).

8. Discussion and outlook

We have explored the concept of Gaussian morphing, namely, controlling the shape of a thin two-dimensional structure by actively modulating the stretching of its mid-surface both in the context of biological systems, and with a view towards applications to engineering devices. We have used the unifying paradigm of Gaussian morphing to rationalize the shape-shifting abilities of some biological organisms and structures (the unicellular predator *Lacrymaria olor*, the euglenid protist *Euglena gracilis*, the $9 + 2$ structure of the eukaryotic flagellum), and to draw a conceptual bridge towards some (either existing or speculative) engineering applications (McKibben artificial muscles, active pellicle surfaces).

One point we have not discussed explicitly is the role of bending stiffness. Indeed, predicting shape on the basis of Gauss theorema egregium means to disregard it entirely. This gives realistic

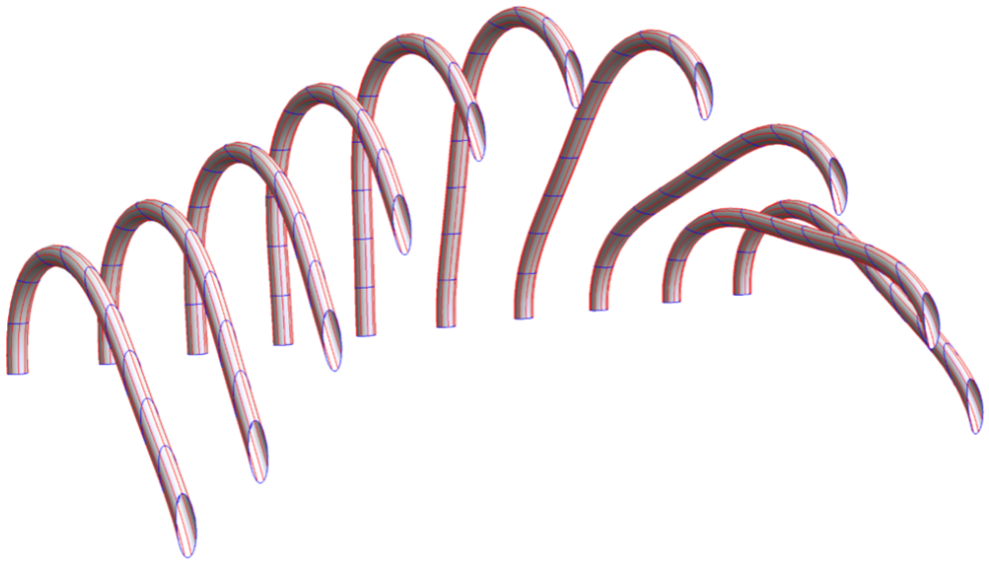

Figure 6: Set of surfaces mimicking several configurations of the axoneme within the flagellar beat of *Chlamydomonas reinhardtii*. Material fibers (microtubules) are shown in red. The deformed configurations of the coordinate lines $v = kL_0/10$, with $k = 0, 1, \ldots, 10$, are shown in blue.

results for very thin, continuous elastic shells when an embeddable metric is prescribed, and the embedding problem has a unique solution. How realistic is this prediction if the metric is not embeddable (non-existence), or if there are multiple embeddings (non-uniqueness), or if there are dissipative (frictional, viscous, poroelastic, plastic,...) internal forces, or external resistive forces due to the presence of a surrounding fluid, or if the thickness is not vanishingly small, or if the structure is actually made up of discrete elements (fibers, strips, joints,...)? These are all very relevant issues, but beyond the scope of this paper. We refer to Arroyo and DeSimone (2014); Noselli et al. (2019a) for a discussion of some of these issues (in particular: regularizing role of bending stiffness in the case of non-uniqueness or non-embeddability; effects of discreteness and specific additional elastic terms induced by torsional and flexural stiffness of the rods when the active surface consists of a discrete network of structural elements rather than of a continuous surface).

Leaving the issue of bending stiffness aside, our analysis shows that even in the simplest setting of Gaussian morphing of axisymmetric shapes, there is a need for a more precise (mathematical) definition of the problem of shape control (both in the so called direct and inverse form). What are the data? And what are the unknowns? When do solutions exist and are they unique? Our simple example summarized in Figure 4, and the comparison between the shape changes exhibited by unicellular organisms (neck extension vs metaboly) show the need of distinguishing clearly between shape control (intrinsic geometric parameters of the target surface), control of the map prescribing how material points are moved (parametrization of the target surface), and mechanism of actuation (the metric tensor of the target surface). In addition, it shows the need of including in the problem formulation a precise description of the way specific material lines are transformed by the morphing principle, *i.e*, a description of the active structures used to enforce the metric changes (the embodiment of the Gaussian morphing principle).

In fact, our concrete examples illustrate how the same shape can be attained with different

metrics, which means different actuation patterns, and with different realizations, which means by inducing different displacements of Lagrangian markers placed on the surface. This is particularly relevant since, in any concrete implementation of the morphing concepts we have described, these Lagrangian markers will be identified with specific material points of the structural elements making up the surface. Their displacement will be the negotiated outcome of the competition between internal forces of actuation and elastic (viscoelastic, plastic, etc. ...) properties resisting conformational changes. In other words, different practical realizations (embodiments) of the same Gaussian morphing scheme will lead to different elastic compliance (deviation form the prescribed metric), different effective bending stiffness competing with (sometimes hindering, sometimes regularizing) the predictions based on the *theorema egregium*. Ultimately, these different embodiments of the same principle will lead to different shape-shifting mechanisms, different realizable and realized shapes, different performance. It is in these details that we expect to find treasures (rather than devils, see Cohen (2004)), be it in the form of a deeper understanding of the inner workings of biological organisms, or in the form of novel mechanisms leading to innovative engineering devices.

Acknowledgments

The concept of morphing surfaces by active pellicle sliding is the subject of a patent application. We gratefully acknowledge the support by the European Research Council through the ERC Advanced Grant 340685-MicroMotility. This paper was completed while ADS was visiting the University of Cambridge as a Visiting Scholar at Pembroke College and a participant to the Newton Institute programme on "The Mathematical Design of New Materials". The hospitality of both Institutions is gratefully acknowledged. The video of a lecture given at the Newton Institute for Mathematical Sciences on the themes of this paper within a workshop celebrating "Women in Materials Science", supported by ESPRC grant number EP/R014604/1, can be found here https://sms.cam.ac.uk/media/2986233/formats. We dedicate this article to prof. J.M. Ball in celebration of his recent birthday.

References

Agostinelli, D., Alouges, F., De Simone, A., 2018. Peristaltic waves as optimal gaits in metameric bio-inspired robots. Frontiers in Robotics and AI 5, 99.

Agostiniani, V., DeSimone, A., Lucantonio, A., Lucic, D., 2018. Foldable structures made of hydrogel bilayers. doi:10.3934/Mine.2018.1.204.

Aharoni, H., Abraham, Y., Elbaum, R., Sharon, E., Kupferman, R., 2012. Emergence of Spontaneous Twist and Curvature in Non-Euclidean Rods: Application to *Erodium* Plant Cells. Physical Review Letters 108, 238106. URL: http://link.aps.org/doi/10.1103/PhysRevLett.108.238106, doi:10.1103/PhysRevLett.108.238106.

Aharoni, H., Sharon, E., Kupferman, R., 2014. Geometry of thin nematic elastomer sheets. Phys. Rev. Lett. 113, 257801. URL: http://link.aps.org/doi/10.1103/PhysRevLett.113.257801, doi:10.1103/PhysRevLett.113.257801.

Dreyfus et al., R., 2005. Microscopic artificial swimmers. Nature 437, 862–865.

Alberts, B., Johnson, A., Lewis, J., Morgan, D., Raff, M., Roberts, K., Walter, P., 2014. Molecular Biology of the Cell, 6th ed. Garland Science.

Alouges, F., DeSimone, A., Giraldi, L., Or, Y., Wiezel, O., 2019. Energy-optimal strokes for multi-link microswimmers: Purcell's loops and Taylor's waves reconciled. New Journal of Physics 21, 043050.

Alouges, F., DeSimone, A., Giraldi, L., Zoppello, M., 2013. Self-propulsion of slender micro-swimmers by curvature control: n-link swimmers. International Journal of Non-Linear Mechanics 56, 132–141.

Alouges, F., DeSimone, A., Heltai, L., 2011. Numerical strategies for stroke optimisation of axisymmetric micro-swimmers. Mathematical Models and Methods in Applied Sciences 21, 361–387.

Arroyo, M., DeSimone, A., 2014. Shape control of active surfaces inspired by the movement of euglenids. J. Mech. Physics Solids 62, 99–112. doi:10.1016/j.jmps.2013.09.017.

Arroyo, M., Milan, D., Heltai, L., DeSimone, A., 2012. Reverse engineering the euglenoid movement. Proc. Nat. Acad. Sciences USA 109, 17874–17879.

Becker, L.E., Koehler, S.A., Stone, H.A., 2003. On self-propulsion of micro-machines at low Reynolds number: Purcell's three-link swimmer. Journal of Fluid Mechanics 490, 15–35.

Camalet, S., Jülicher, F., 2000. Generic aspects of axonemal beating. New Journal of Physics 2, 24.

do Carmo, M.P., 1976. Differential Geometry of curves and surfaces. Paperback.

Caruso, A., Cvetkovic, A., Lucantonio, A., Noselli, G., DeSimone, A., 2018. Spontaneous morphing of equibiaxially pre-stretched elastic bilayers: the role of sample geometry. Int. J. Mechanical Sciences 149, 481–486. doi:10.1016/j.ijmecsci.2017.08.049.

Cicconofri, G., DeSimone, A., 2015. A study of snake-like locomotion through the analysis of a flexible robot model. Proc. R. Soc. A 471, 20150054. doi:10.1098/rspa.2015.0054.

Cicconofri, G., DeSimone, A., 2016. Motion planning and motility maps for flagellar microswimmers. Eur. Phys. J. E 39, 72. doi:10.1140/epje/i2016-16072-y.

Cicconofri, G., DeSimone, A., 2019. Modelling biological and bio-inspired swimming at microscopic scales: Recent results and perspectives. Computers and Fluids 179, 799–805. doi:10.1016/j.compfluid.2018.07.020.

Cohen, J., 2004. Mathematics is Biology's next microscope, only better; Biology is Mathematics' next Physics, only better. PLoS Biology 2, e439. doi:10.1371/journal.pbio.0020439.

Coyle, S., Flaum, E., Li, H., Krishnamurthy, D., Prakash, M., 2018. Coupled active systems encode emergent behavioral dynamics of the unicellular predator Lacrymaria olor. BiorXiv doi:10.1101/406595.

DeSimone, A., 2018. Spontaneous bending of pre-stretched bilayers. Meccanica 53, 511–518. doi:10.1007/s11012-017-0732-z.

DeSimone, A., Gidoni, P., Noselli, G., 2015. Liquid crystal elastomer strips as soft crawlers. Journal of the Mechanics and Physics of Solids 84, 254–272.

DeSimone, A., Guarnieri, F., Noselli, G., Tatone, A., 2013. Crawlers in viscous environments: linear vs non-linear rheology. International journal of non-linear mechanics 56, 142–147.

Drescher, K., Goldstein, R., Michel, N., Polin, M., Duval, I., 2010. Direct measurement of the flow field around swimming microorganisms. Physical Review Letters 105, 168101.

Feng, J., Cho, S., 2014. Mini and micro propulsion for medical swimmers. Micromachines 5, 97–113.

Feynman, R., 1960. There's plenty of room at the bottom: An invitation to enter a new field of Physics. Engineering and Science 23, 22–36.

Freund, L., 2000. Substrate curvature due to thin film mismatch strain in the nonlinear deformation range. Journal of the Mechanics and Physics of Solids 48, 1159–1174. doi:10.1016/S0022-5096(99)00070-8.

Gaffney, E., Gadelha, H., Smith, D., Blake, J., Kirkman-Brown, J., 2011. Mammalian sperm motility: Observation and theory. Annu. Rev. Fluid Mech. 43, 501–528.

Goldstein, R.E., 2015. Green algae as model organisms for biological fluid dynamics. Annu. Rev. Fluid Mech. 47, 343–375.

Kim, J., Hanna, J.a., Byun, M., Santangelo, C.D., Hayward, R.C., 2012. Designing responsive buckled surfaces by halftone gel lithography. Science 335, 1201–1205. URL: http://www.ncbi.nlm.nih.gov/pubmed/22403385, doi:10.1126/science.1215309.

Kim, S., Laschi, C., Trimmer, B., 2013. Soft robotics, a bio-inspired evolution in robotics. Trends in Biotechnology 31, 287–294.

Klein, Y., Efrati, E., Sharon, E., 2007. Shaping of elastic sheets by prescription of non-Euclidean metrics. Science 315, 1116–1120. doi:10.1126/science.1135994.

Lauga, E., Powers, T.R., 2009. The hydrodynamics of swimming microorganisms. Reports on Progress in Physics 72, 096601.

Lighthill, J., 1975. Mathematical biofluiddynamics. Society for Industrial and Applied Mathematics, Philadelphia, Pa. .

Lin, J., Nicastro, D., 2018. Asymmetric distribution and spatial switching of dynein activity generates ciliary motility. Science 360, eaar1968.

Lindemann, C.B., Lesich, K.A., 2010. Flagellar and ciliary beating: the proven and the possible. J Cell Sci 123, 519–528.

Machin, K., 1958. Wave propagation along flagella. Journal of Experimental Biology 35, 796–806.

Menciassi, A., Accoto, D., Gorini, S., Dario, P., 2006. Development of a biomimetic miniature robotic crawler. Autonomous Robots 21, 155–163.

Modes, C.D., Warner, M., 2015. Negative Gaussian curvature from induced metric changes. Phys. Rev. E 92, 010401. URL: http://link.aps.org/doi/10.1103/PhysRevE.92.010401, doi:10.1103/PhysRevE.92.010401.

Mostajeran, C., 2015. Curvature generation in nematic surfaces. Phys. Rev. E 91, 062405. URL: http://link.aps.org/doi/10.1103/PhysRevE.91.062405, doi:10.1103/PhysRevE.91.062405.

Noselli, G., Arroyo, M., DeSimone, A., 2019a. Smart helical structures inspired by the pellicle of euglenids. Journal of the Mechanics and Physics of Solids 123, 234–246. doi:10.1016/j.jmps.2018.09.036.

Noselli, G., Beran, A., Arroyo, M., DeSimone, A., 2019b. Swimming Euglena respond to confinement with a behavioural change enabling effective crawling. Nature Physics 15, 496–502. doi:10.1038/s41567-019-0425-8.

Noselli, G., DeSimone, A., 2014. A robotic crawler exploiting directional frictional interactions: experiments, numerics and derivation of a reduced model. Proceedings of the Royal Society A: Mathematical, Physical and Engineering Sciences 470, 20140333.

Oriola, D., Needleman, D., Brugues, J., 2018. The physics of the metaphase spindle. Annual Review of Biophysics 47, 655–673.

Ornes, S., 2017. Medical microrobots have potential in surgery, therapy, imaging, and diagnostics. Proc. Nat. Acad. Sciences USA 114, 12356–12358.

Pellegrino, S., 2001. Deployable structures. Springer-CISM International Centre for Mechanical Sciences.

Pellegrino, S., 2018. Space solar power: a new beginning. https://www.youtube.com/watch?time_continue=7&v=em8T1nOL0tM. [Online; accessed 14-May-2019].

Purcell, E.M., 1977. Life at low Reynolds number. Am. J. Phys 45, 3–11.

Rossi, M., Cicconofri, G., Beran, A., Noselli, G., DeSimone, A., 2017. Kinematics of flagellar swimming in euglena gracilis: Helical trajectories and flagellar shapes. Proceedings of the National Academy of Sciences USA doi:10.1073/pnas.1708064114.

Santangelo, C., 2011. Buckling thin disks and ribbons with non-Euclidean metrics. Europhysics Letters 86, 34003.

Sawa, Y., Urayama, K., Takigawa, T., DeSimone, A., Teresi, L., 2010. Thermally driven giant bending of liquid crystal elastomer films with hybrid alignment. Macromolecules 43, 4362–4369. doi:10.1021/ma1003979.

Shahaf, A., Efrati, E., Kupferman, R., Sharon, E., 2011. Geometry and mechanics in the opening of chiral seed pods. Science 333, 1726–1730. doi:10.1126/science.1203874.

Shapere, A., Wilczeck, F., 1989. Geometry of self-propulsion at low Reynolds number. Journal of Fluid Mechanics 198, 557–585.

Taylor, G.I., 1951. Analysis of the swimming of microscopic organisms. Proceedings of the Royal Society of London A: Mathematical, Physical and Engineering Sciences 209, 447–461.

Taylor, J., 2019. Bimetal kettle switch. http://www.johnctaylor.com/my-world/inventions/. [Online; accessed 14-May-2019].

Timoshenko, S., 1925. Analysis of bi-metal thermostats. J. Optical Soc. Am. 11, 233–255.

Tondu, B., 2012. Modelling of the McKibben artificial muscle: A review. Journal of Intelligent Material Systems and Structures 23, 225–253. URL: http://jim.sagepub.com/content/23/3/225.abstract, doi:10.1177/1045389X11435435.